System Design Optimization for Multimegawatt Space Nuclear Power Applications

M. S. El-Genk,* A. G. Parlos,† J. M. McGhee,‡ and S. Lapin‡
University of New Mexico, Albuquerque, New Mexico
and
D. Buden§ and J. Mims¶
Science Applications International Corporation, Albuquerque, New Mexico

The results of a design and optimization study of the Pellet Bed Reactor System Concept (PBRSC) for meeting the multimegawatt power needs of some Strategic Defense Initiative (SDI) missions during both alert and burst modes of operation are presented. The power system consists of four modules, each capable of providing up to 165 MWe during the burst mode and 3.3 MWe during the alert mode. This modular approach provides redundancy, with low-mass penalty, and it increases the power plant's survivability by requiring an attack force to destroy many independent power modules. Results indicate that the specific power of a hydrogen-cooled Pellet Bed Reactor/potassium Rankine cycle module (3.8 kWe/kg) is superior to a closed-loop Brayton cycle module (3.1 kWe/kg), but comparable with an open-loop Brayton cycle module (3.8 kWe/kg). The comparison established that the closed-loop Brayton cycle module needs about 10 times higher compressor power than the Rankine cycle module, resulting in a lower specific power. Additionally, the savings in the radiator mass resulting from the higher efficiency of the closed-loop Brayton cycle module (20% vs 17% for Rankine cycle module) is offset by the higher heat rejection load caused by the higher reactor thermal power to compensate for the higher compressor power. Analysis also established that the combined masses of the hydrogen tank and the attached refrigeration unit of the open-loop Brayton cycle module favorably compare with those of the radiator and the vapor generator for the Rankine cycle module.

Nomenclature

A = surface area, average flow area (m^2)
C_p = specific heat capacity (J/kg·K)
D_p = diameter of fuel element (m)
h = heat-transfer coefficient ($W/m^2 \cdot K$)
L = length of flow path (m)
$\dot{m}$ = mass flow rate (kg/s)
Nu = Nusselt number
P = power (W), pressure (Pa)
Pr = Prandtl number
ΔP = pressure loss (Pa)
$\bar{p}$ = as fabricated fuel porosity
Q = thermal energy (J)
$\bar{q}'''$ = average volumetric heat-generation rate (W/m^3)
R = radius of vapor generator vessel (m)
Re = Reynolds number
Re_m = modified Reynolds number $[\rho \bar{V} D_p / \bar{\mu}(1 - \varepsilon_{core})]$
S = pitch of vapor generator tube (m)
S_m = 1/3 of ultimate yield strength (Pa)
T = temperature (K)
$\bar{T}$ = average temperature (K)
V = volume (m^3)
$\bar{V}$ = average flow velocity (m/s)
W = mechanical work (J/kg)
ε = surface emissivity, void fraction
η = thermodynamic efficiency (%)
$\bar{\mu}$ = average dynamic viscosity (kg/s·m)
ρ = density (kg/m^3)
σ = Stefan-Boltzmann constant ($W/m^2 \cdot K^4$)

Subscripts

amb = ambient
b = coolant bulk
c = graphite, compressor
cycle = energy conversion cycle
core = reactor core
e = electric
ex = core exit
EM = electromagnetic pump
FE = fuel element
G = electric generator
HX = vapor generator
HP = high-pressure turbine
in = core inlet
LP = low-pressure turbine
max = fuel element maximum
pipes = primary loop piping
plant = power module
R = heat rejection
RH = vapor generator reheater
rad = radiator
s = fuel element surface
sur = radiator surface
T = turbine
t = total
th = thermal
uc = uranium carbide
1 = core inlet channel
2 = core exit channel

Received Sept. 28, 1987; revision received March 3, 1988. This paper is declared a work of the U.S. Government and is not subject to copyright protection in the United States.

*Professor and Director of the Institute for Space Nuclear Power Studies, Department of Chemical and Nuclear Engineering.

†Research Associate, Institute for Space Nuclear Power Studies, Department of Chemical and Nuclear Engineering; currently Assistant Professor, Nuclear Engineering Department, Texas A & M University, College Station, Texas.

‡Graduate Student and Research Assistant, Institute for Space Nuclear Power Studies, Department of Chemical and Nuclear Engineering.

§Senior Program Manager.

¶Senior Scientist.

I. Introduction

FOR Strategic Defense Initiative (SDI) missions, the operating modes and the concomitant electric power needs include: 1) station-keeping mode, requiring continuous power in the tens to hundreds of kWe for up to seven years, 2) standby/alert mode, requiring continuous power in the tens of megawatts for up to one year, and 3) burst mode, requiring hundreds of megawatts for tens to thousands of seconds. The SP-100 multihundred kilowatt program centers on the low-power range (stationkeeping mode)[1]; however, the anticipated power ranges for the alert and the burst modes will require innovative and revolutionary approaches to power system design. These multimodal power systems should possess low specific mass and volume as well as high reliability and plant survivability.

The specific objectives of this study were to 1) analyze and optimize the design of a power module utilizing the Pellet Bed Reactor (PBR) concept for meeting the multimegawatt power needs of the SDI missions during both the alert and burst modes, and 2) compare different module designs for maximum specific power. The power modules compared in this study include gas-cooled PBR/liquid-metal Rankine cycle, gas-cooled PBR/closed-loop Brayton cycle, and PBR/open-loop Brayton cycle. The study also focused on analyzing the effects of gas coolant type (helium or hydrogen), the turbine inlet temperature, and the pressures of the primary and secondary loops on the module's performance and specific power.[2,3] Finally, key research and development issues encountered during the study are discussed; and some possible solutions are recommended.

Description of Pellet Bed Reactor System Concept

The PBR concept is a new and innovative concept built on an established pebble bed terrestrial technology base.[4] This concept employs a fast-flux, hydrogen-cooled reactor fueled with graphite-coated, spherical fuel elements, thus eliminating the need for internal core structure. Reactor fueling can be performed at the launch facility or in orbit, and refueling can be accomplished in orbit as needed to extend the power system's lifetime for up to 30 years. To enhance operational reliability, the power system has four identical power modules; three modules can be used in the duty cycle while one module is a standby, or all four modules can operate at partial power. This modular approach allows flexibility in the design, assembly, and deployment of the system, and provides redundancy by incorporating additional power modules rather than built-in redundancies in the power plant. The modular approach also increases the power plant's survivability by requiring an attack force to destroy many independent power modules.

Each power module, equipped with a pellet bed, hydrogen-cooled reactor, potassium Rankine cycle for the energy conversion, and a deployable radiator for heat rejection, produces 165 MWe during the burst mode and up to 3.5 MWe during the alert mode. During the alert mode, the deployable radiator (specific mass of 1.4 kg/m^2) is protected from space debris and meteorites by being folded up inside an armored compartment.[5] The outer surface of this compartment (specific mass of 14 kg/m^2) provides heat rejection during the alert mode. This flexible radiator arrangement minimizes the mass of the armor needed and keeps the deployable radiator temperature high enough for rapid deployment during the burst mode.

The design goal of the PBR power modules is to minimize the overall power system mass while maintaining a high degree of reliability. In order to achieve the first of these goals, the design optimization studies focused on the following: 1) selecting the fuel temperature for minimum core size and mass, 2) optimizing the fuel element diameter for high-heat transfer and low-pressure losses, 3) selecting the reactor core height-to-diameter ratio for low-pressure losses and small compressor size, 4) selecting the operating pressures and the working fluids in the primary and secondary loops for minimum radiator mass, and 5) shortening the transition time from the alert mode to the burst mode by keeping the operating pressures and temperatures of the energy conversion-secondary loop the same during both modes. Therefore, the power output is altered by changing only the reactor power and the potassium mass flow rate in the secondary loop.

Pellet Bed Reactor Design

Figure 1 presents a cross-sectional view of the PBR along with the zoning scheme used in the neutronics calculations. As this figure indicates, hydrogen gas enters the reactor through the outer annulus, flows radially through the core, then exits through the central channel. This arrangement sufficiently cools the pressure vessel while reducing the pressure losses in the core. The temperature of the reflector is kept low by thermally insulating the top, bottom, and radial Be_2C reflectors using a high-temperature multifoil insulation. The gas enters the core through a Mo-10Re frit and exits through an ASTAR-811C frit. The openings of these frits are sized to provide an equal pressure drop in the core, irrespective of axial location. The reactor vessel is made of MO-10Re mixed with high-temperature ceramic Nicalon fibers.[3] The Nicalon fibers not only add strength but also result in a thinner wall and lighter mass of the pressure vessel. The core is surrounded by a total of 26, 11-cm-diam segmented B_4C/Be_2C control drums and a Be_2C reflector. The reactor power level is altered by rotating the drums inward or outward. In order to prevent immersion recriticality, the core is equipped with eight 4-cm-diam control rods located 19 cm from the center of the core.

Fuel Element Design

The PBR utilizes spherical fuel elements that are 1 cm in diameter and contain coated fuel microspheres dispersed in a graphite matrix. As the schematic in Fig. 2 shows, the fuel

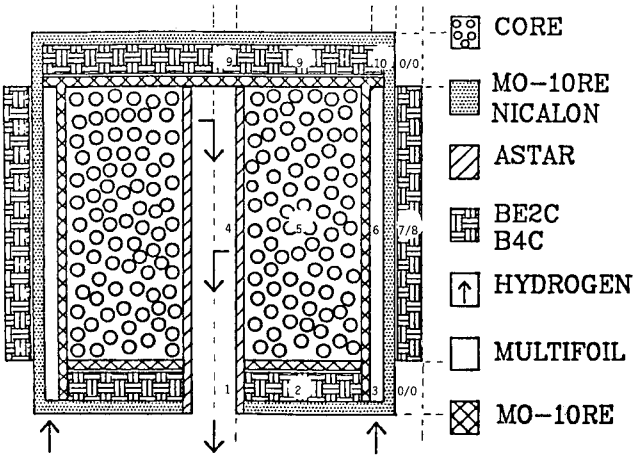

Fig. 1. Cross-sectional view of the Pellet Bed Reactor configuration with neutronically homogeneous zones.

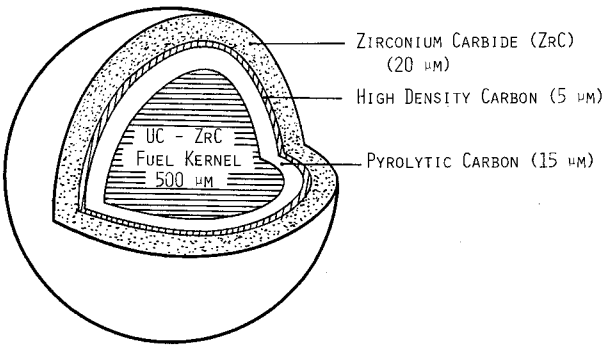

Fig. 2. Cross-sectional view of a fuel microsphere.

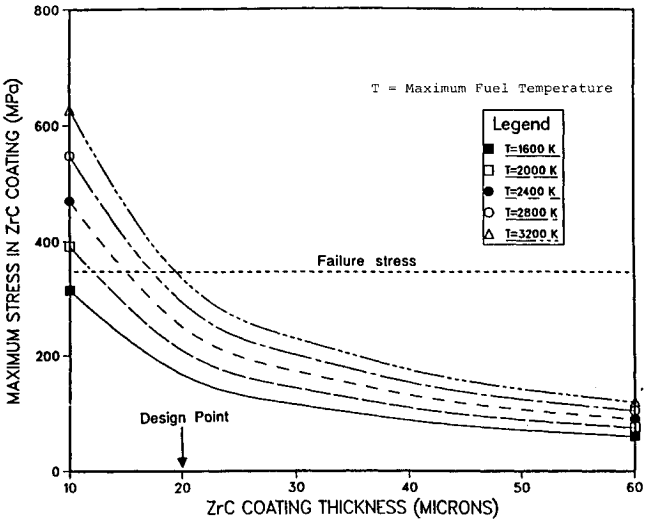

Fig. 3. Effect of maximum fuel temperature on the induced stress in the ZrC coating.

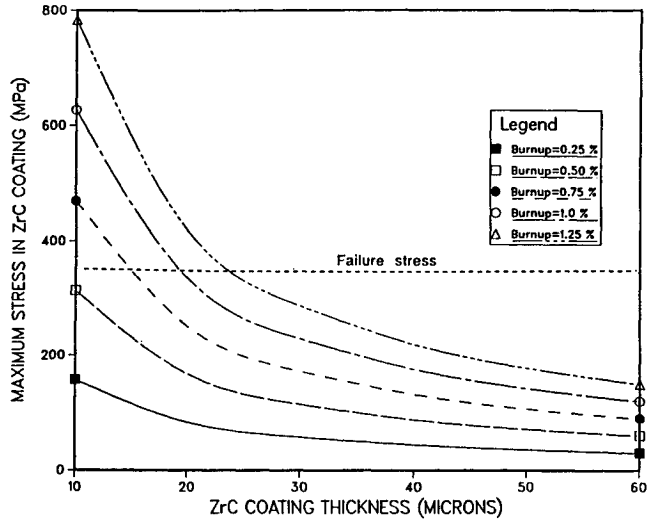

Fig. 4. Effect of fuel burnup on the maximum stress induced in the ZrC coating.

microsphere consists of a UC-ZrC fuel kernel, 500 μm in diameter, with a triple coating:[6] inner coating of low density, Pyrolytic graphite (PyC), 15 μm thick; intermediate coating of high-density graphite, 5 μm thick; and ZrC outer coating, 20 μm thick. The UC-ZrC fuel allows higher operating temperatures because increasing the ZrC percentage increases the fuel's melting point (up to 3600 K). The Pyrolytic Carbon (Pyc) coating accommodates the fission products' recoil and partially accommodates the fission gases,[7] while the high-density graphite strengthens the coating and suppresses the absorption of HCl acid during the ZrC coating process. Finally, the ZrC outer coating prevents fission gas release from the microspheres. The combination of graphite and ZrC had a comparable thermal expansion coefficient to that of the fuel and a high thermal conductivity to remove the generated heat effectively, and is strong enough to accommodate stresses due to fission product buildup.[8,9] The thermal stresses were considered negligible since the coating process of the microspheres will be performed at almost the same temperature as the reactor operating temperature. The stresses caused by the buildup of fission gases and volatiles in the fuel microsphere were calculated as functions of the as fabricated porosity of the fuel and the PyC coating.[8] Because of the absence of data at high temperatures (1800–3000 K), a conservative estimate for the ZrC fuel coating failure stress of 350 MPa was used.[10] The parameters for the stress analyses of the ZrC coating are: fuel burnup at 1.0 atom %, radius of fuel kernel of 250 μm, maximum fuel temperature of 3200 K, PyC coating thickness of 20 μm, as fabricated fuel density of 95% TD, and as fabricated PyC density of 1.6 Kg/m^3.

As shown in Fig. 3, increasing the maximum fuel temperature increases the pressure buildup in the fuel kernel and, therefore, the induced stresses in the ZrC coating. Conversely, increasing the ZrC coating thickness causes the stress to decrease rapidly up to a thickness of 20 μm; beyond this point, increasing the ZrC coating thickness reduces the stress at a much slower rate. This behavior is due to the fact that the induced stresses are inversely proportional to the thickness of the coating raised to the third power.[8] The results in Fig. 4 also show that the induced stress in the ZrC coating increases with increasing fuel burnup because of the higher accumulation of fission products. For a ZrC coating thickness of 20μm, the maximum possible fuel burnup without failing the coating is 1 atom %; this burnup is slightly higher than the value expected in the PBRSC at the end of a 1-yr operation in the alert mode (0.8 atom %). This low burnup is a consequence of the core sizing being governed by thermal hydraulics rather than neutronics considerations. The choice of the 500 μm for the kernel radius was determined based on reactor core neutronics and thermal-hydraulics considerations. Smaller fuel kernel radius increases the coating-to-fuel volume ratio, resulting in an effective multiplicative factor that is less than 1. In addition, reducing the fuel kernel radius increases the core pressure losses and the power requirement for the compressor, causing the reactor thermal power to increase and the system specific power to decrease. Because the fuel operating temperature during the alert mode (1850 K) is lower than that expected during the burst mode (3000–3200 K), the selected design parameters of the fuel microspheres will guarantee the integrity of the fuel microsphere in both the burst and alert modes. To ensure that the maximum fuel temperature would not exceed 90% of its melting point during the burst and alert modes of operations, the content of ZrC in the fuel kernel was selected to be 23%.

Other important considerations in the fuel element design were the materials compatibility issues,[10] namely, 1) the hydrogen-graphite reaction at elevated temperatures, and 2) the diffusion of uranium through the ZrC coating. To eliminate the first problem, the fuel elements were coated with a thin layer ($\sim$5 μm) of ZrC. With regard to the second problem, experimental evidence shows that when ZrC in contact with UC fuel is heated to about 2000 K, uranium migrates from the fuel kernel to the ZrC layer. This migration causes fissioning in the ZrC layer that, subsequently, leads to its destruction and ultimately the failure of the fuel microspheres. The rate of uranium migration and its penetration distance into the ZrC coating are strong functions of the temperature and the operation time at that temperature. However, since the alert mode operating temperature will be 1850 K for one year, no significant uranium diffusion into the ZrC coating is expected; uranium migration might be an issue during the burst mode because the operating temperature could be as high as 3000 K.

Primary Loop Thermal Hydraulics and Energy Conversion Loop Analyses

During operation, the thermal energy is removed from the reactor core and transferred through a vapor generator to a liquid potassium secondary loop. Liquid potassium enters the vapor generator where it is converted into vapor and then the vapor is superheated. The superheated potassium vapor expands through a high-pressure turbine; it is then reheated to the same superheated temperature before entering the low-pressure turbine. The potassium vapor expands through the low-pressure turbine, then exits to the condenser where waste heat is rejected through the radiator into space. The potassium

condensate is recirculated using an electromagnetic (EM) pump. The circulation of the hydrogen gas in the primary loop is accomplished by a compressor that is mounted on a common shaft with the turbine generator.

A thermal-hydraulics model for the primary loop was developed based on a lumped parameter analysis of the conservation equations of mass, momentum, and energy. This model was then coupled to the secondary-loop energy conversion model. The following assumptions and design choices were made in the development of the thermal hydraulics and the energy conversion models: 1) the properties of the subcooled potassium entering the vapor generator are set equal to those of saturated liquid potassium at the same temperature; 2) the pipings, reactor vessel, vapor generator, and other system components are well insulated; 3) to reduce structural vibrations resulting from higher coolant velocities, the hydrogen's inlet and exit velocities are set equal to half of the sonic speed at the respective temperatures; 4) pressure losses in the primary side of the vapor generator are set equal to the total core pressure losses; 5) the pressure losses in the primary-loop piping are set equal to 20% of the total core pressure losses; 6) the materials properties in the primary and secondary loop are allowed to vary with temperature; and 7) the turbine efficiency is taken to be 90%, EM pump efficiency is 20%, and the compressor and electric generator efficiencies are 95 and 99%, respectively.

The pressure losses in the inlet and exit channels of the reactor core are modeled as those for flow through a circular pipe with the appropriate equivalent hydraulic diameter. The pressure losses in the core are calculated using von Kármán correlation for packed particle beds[12]:

$$\Delta p_{\text{core}} = 4K_{ef}\frac{\rho \bar{V}^2}{2}\frac{L}{D_p} \tag{1}$$

where

$$K_{ef} = \left(\frac{1-\varepsilon_{\text{core}}^3}{\varepsilon_{\text{core}}^3}\right) f \tag{2}$$

and

$$f = \begin{cases} 75/Re_m, & \text{for } Re_m < 10 \\ 0.875 + 75/Re_m, & \text{for } 10 \le Re_m < 1000 \\ 0.875, & \text{for } Re_m \ge 1000 \end{cases} \tag{3}$$

The heat-transfer coefficient in the core is calculated from the following correlation[13]:

$$\varepsilon_{\text{core}}\frac{Nu}{Pr^{1/3}Re} = \frac{2.876}{Re} + \frac{0.3023}{Re^{0.35}} \tag{4}$$

where all fluid properties are evaluated at the coolant's average bulk temperature $\bar{T}_b$. This temperature is related to the fuel element's average surface temperature $\bar{T}_s$, as

$$\bar{T}_b = \bar{T}_s - \frac{D_p}{6}\frac{\bar{q}'''_{\text{core}}}{(1-\varepsilon_{\text{core}})h_c} \tag{5}$$

The fuel element maximum temperature is related to its surface temperature as

$$\bar{T}_{\max} = \bar{T}_s + \frac{D_p^2}{12}\frac{\bar{q}'''_{\text{core}}}{(1-\varepsilon_{\text{core}})}\frac{1}{k_{FE}} \tag{6}$$

The effective thermal conductivity of the fuel element is given as[11]

$$k_{FE} = k_c\left\{\frac{2+(k_{uc}/k_c)-2\varepsilon_{FE}[1-(k_{uc}/k_c)]}{2+(k_{uc}/k_c)+\varepsilon_{FE}[1-(k_{uc}/k_c)]}\right\} \tag{7}$$

where

$$k_{uc} = k_{uc}^{TD}\left(\frac{1-\bar{p}}{1+\bar{p}}\right) \tag{8}$$

Table 1 Comparison of the operating parameters and masses of the different power module configurations (all masses in metric tons)

	Burst/alert closed Rankine[a] (H_2/K)	Burst/alert closed Rankine[a] (H_e/K)	Burst/alert closed Brayton[b] (H_2)	Burst/alert closed Brayton[a] (H_2)	Burst open Brayton/[b,c] alert closed Rankine (H_2/K)	Burst open Brayton/[a,c] alert closed Rankine (H_2/K)
Core coolant exit temp. (K)	2278/1818	2831/2157	2278	1800	2278/1818	1800/1620
Core coolant inlet temp. (K)	1290/1730	1323/1801	1290	1153	30/1730	30/1530
Radiator surface temp. (K)	1116	1112	1093	863	——/1116	——/920
Hot fuel element C.L. temp. (K)	3000/1840	3395/2242	3000	2522	3000/1840	2522/1642
Primary-loop system pressure (MP_a)	12	12	12	12	1/12	1/12
Secondary-loop system pressure (MP_a)	0.84	0.84	——	——	——/0.84	——/0.84
Turbine inlet temp. (K)	1800	1800	2278	1800	2278/1800	1800/1600
Core thermal power (MW_{th})	983/28	1214/254	835/17	832/17	379/28	379/33
Plant efficiency (%)	17/12	14/1.3	20	20	44/12	44/10
Compressor power (MW_{th})	52/3	111/62	510/10	507/10	0/3	0/4
Turbine power (MW_{th})	212/7	275/66	676/13	674/13	166.7/7	166.7/3
Rejected power (MW_{th})	816/25	1047/251	668/14	665/14	212/25	212/30
Electric power (MW_{th})	165/3.3	165/3.3	165/3.3	165/3.3	165/3.3	165/3.3
Reactor vessel mass	4	4	4	4	6	4.5
Compressor mass	2	4	13	13	0.3	0.3
Heat exchanger mass	11	12	——	——	1	1
Turbines mass	5	7	15	15	6	6
Liquid metal pump mass	0.2	0.1	——	——	0.01	0.01
Radiators mass (Burst and Alert)	18	26	17	39	5	5
Liquid hydrogen tank and refrigeration unit mass	——	——	——	——	22	29
Shield mass	4	4	4	4	4	4
Total mass	44	57	53	75	44	50
Specific power (KW_e/kg)	**3.8**	2.9	3.1	2.2	**3.8**	3.3

[a]Turbine inlet temperature = 1800 K. [b]Turbine inlet temperature = 2278 K. [c]2000 s of operation.

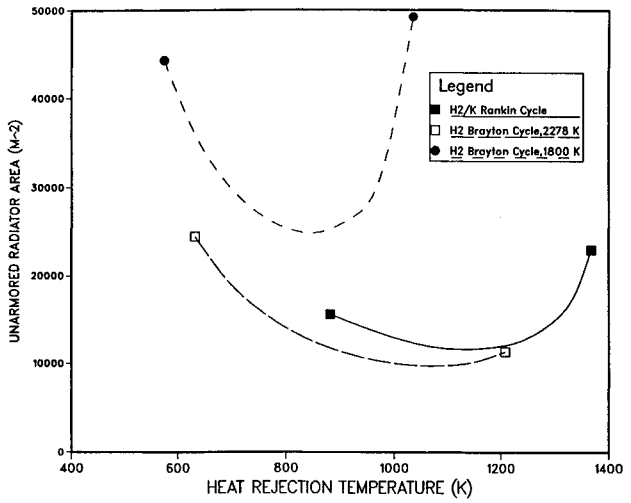

Fig. 5. Optimizations of the radiator surface area for H_2/K Rankine cycle module and hydrogen closed-loop Brayton cycle module.

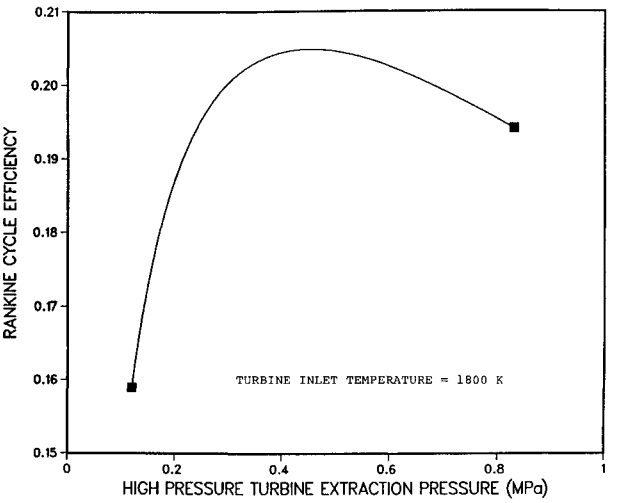

Fig. 6. Effect of high-pressure turbine extraction pressure of the potassium Rankine cycle efficiency.

The Rankine cycle conversion efficiency and that of the overall plant are calculated using the following expressions[14]:

$$\eta_{\text{cycle}} = \left(\frac{P_T}{P_{th} + P_c}\right) = \frac{(W_{HP} + W_{LP} - W_{EM})}{(P_{th} + P_c)} \tag{9}$$

and

$$\eta_{\text{plant}} = \left(\frac{P_e}{P_{th}}\right) = \left(\frac{P_T - P_c}{P_{th}}\right) = \eta_G\left[\eta_{\text{cycle}} - (1 - \eta_{\text{cycle}})\frac{P_c}{P_{th}}\right] \tag{10}$$

where

$$P_{th} = \bar{q}''_{\text{core}} V_{\text{core}} = \dot{m} C_p (T_{\text{ex}} - T_{\text{in}}) \tag{11}$$

The electric power output and the waste heat rejection are given as

$$P_e = \eta_{\text{plant}} P_{\text{th}} \tag{12}$$

and

$$P_R = (1 - \eta_{\text{plant}}) P_{\text{th}} = \varepsilon \sigma A_{\text{rad}} (T^4_{\text{Sur}} - T^4_{\text{amb}}) \tag{13}$$

The final selection of the potassium Rankine cycle for the PBR power modules was based on the results of a comparative analysis between the closed-loop Brayton cycle (with hydrogen or helium as the working fluid) and the liquid-metal Rankine cycle (with lithium or potassium as the working fluid), coupled to a gas-cooled PBR with a hydrogen or a helium coolant (see Table 1). The results of Rankine cycle analysis revealed that to minimize the radiator mass, a potassium working fluid should be used because it has higher vapor pressure than lithium. Also, for a minimum power module mass, a hydrogen/potassium system is superior to a helium/potassium system because hydrogen has a higher heat capacity than helium. As shown in Fig. 5, a hydrogen/potassium system produces the highest radiator temperature, but a slightly higher radiator area than the hydrogen closed-loop Brayton cycle where the turbine inlet temperature in Brayton cycle is taken to be equal to the reactor core exit temperature in the potassium Rankine cycle system (2278 K). When the turbine inlet temperature in the Brayton cycle is the same as that in the potassium Rankine cycle (1800 K), the maximum radiator area (2300 m^2) will be much higher, and the radiator surface temperature (900 K) will be much lower than those for potassium Rankine cycle (1000 m^2 and 1180 K, respectively). These results clearly demonstrate that a significant saving in the radiator mass can be realized with potassium Rankine cycle.

Figure 6 demonstrates that increasing the extraction pressure of the high-pressure turbine, increases the potassium Rankine cycle's conversion efficiency, which reaches a maximum of 20.3% at about 0.43 MPa. Beyond this point, increasing the high-pressure turbine extraction pressure decreases the cycle efficiency. This effect occurs because lowering the extraction pressure below 0.43 MPa increases the reheater's heat demand and, subsequently, the reactor thermal power faster than the associated increase in the turbine's mechanical work, causing the cycle efficiency to decrease. Conversely, increasing the extraction pressure beyond 0.43 MPa lowers the reheater's heat demand and reduces the turbine's mechanical work, causing the cycle efficiency to decrease. At an extraction pressure of 0.43 MPa, however, the increase in the reheater's heat demand results in a faster increase in the turbine's mechanical work, causing the cycle efficiency to peak at 20.3%

Reactor Core Neutronics Analysis

The reactor core neutronics analyses, performed using the TWODANT neutronics code[15] and nine neutron energy groups, evaluated the effects of changes in various core parameters such as the core height and diameter, the fuel density, the graphite matrix volume fraction on the k effective, the neutron flux spectrum, the core control, and the water immersion criticality. The graphite matrix fraction is defined as the volume ratio of the graphite to the total volume of fuel and the graphite in the fuel element. The zoning scheme used in the neutronic analysis is shown in Fig. 1. Results demonstrated that the reactor core has a soft fast neutron spectrum (peak neutron energy of 1–50 Kev, depending on the value of the graphite matrix volume fraction). Reactor's neutron spectrum showed little sensitivity to changes in the core diameter (from 48 to 86 cm) or in the as fabricated fuel density (from 85 to 100% of theoretical density). However, the neutron's energy spectrum was very sensitive to changes in the graphite matrix fraction.[2] Increasing the graphite matrix fraction results in a softer neutron spectrum with a higher microscopic fission cross section; therefore, it causes the k effective to increase. At the same time, a high graphite matrix fraction reduces the amount of fuel in the core, thus reducing the k effective. However, the last effect dominates, causing the k effective to decrease rapidly as the graphite matrix fraction is increased.

The neutronics analyses also indicated that eight B_4C control rods (4 cm in diameter) located symmetrically 19 cm from the

core centerline combined with a central B_4C plug, can keep the reactor subcritical during a water immersion accident (k effective = 0.940). During normal operation, however, the control drums alone can sufficiently control the reactor (k effective = 1.07 and 0.923 with the B_4C drums turned outward and inward respectively). Results also showed that after one year of continuous operation in the alert mode at 3.3 MWe per module, the maximum fuel burnup expected is 0.8 atom %; in contrast, the fuel burnup caused by operating in the burst mode is negligible.

Vapor Generator Design

As indicated earlier, the vapor generator in the PBR power module provides superheated potassium for both the high- and low-pressure turbines. To minimize the possibilities of flow instabilities, the pressure losses in the primary side of the vapor generator were limited to 10% of primary loop pressure losses, and the pressure losses in the secondary side were limited to 20% of the secondary loop pressure losses. The boiler tube pitch was selected to minimize the pressure losses in the primary and secondary loops, and satisfy the above pressure losses criteria. Additional design goals for the vapor generator included assuring efficient two-phase separation in a microgravity environment, and minimizing the vapor generator mass.[2,3] As shown in Fig. 7, the vapor generator consists of a once-through boiler/superheater to provide superheated vapor for the high-pressure turbine, and a separate reheater to provide superheated vapor for the low-pressure turbine. Both the boiler/superheater and the reheater units utilize a counterflow configuration to maximize heat transfer. Flow on the shell side parallels the vapor generator tubes, and thus minimizes pressure losses. The thin twisted ribbons inserted inside the boiler tubes induce a centrifugal force for efficient two-phase separation. The shell, the tubes, and the reheater of the vapor generator are all constructed from a fiber reinforced refractory metal (ASTAR-1611C) for maximum strength and lower mass at the system's high operating temperatures (2800–2300 K).

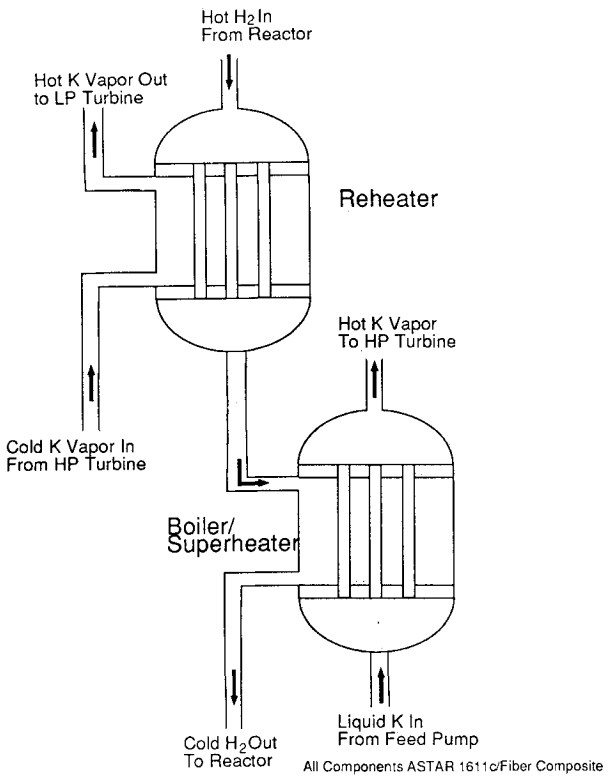

Fig. 7. Line diagram of the vapor generator-superheater unit.

The Dittus-Bolter heat-transfer correlation was used to calculate the heat-transfer coefficient on the gas side, and the potassium liquid heat-transfer coefficient on the tube side was calculated using the Lyons-Martinelli correlation.[16] In the superheater and the reheater, the Dittus-Bolter correlation was also used to calculate the heat-transfer coefficient for the potassium vapor flow. Because of the lack of data and applicable correlations, no attempt was made to determine the critical heat flux for the liquid-metal flow. The Darcy-Weisbach equation was used for all single-phase pressure loss calculations; however, to account for the two-phase pressure losses in the boiler, the pressure losses for saturated liquid were multiplied by an arbitrary two-phase friction multiplier of 80. The masses of the vapor generator vessel and of the tubes were estimated using the thin shell model,[17] and the thickness of vessel header was calculated using the following relations[18]:

$$\text{Header wall thickness} = \left(\frac{PR^2}{S_m}\right)(2 + 9.11s^{-4.79}) \quad (14)$$

A parametric analysis of the vapor generator design indicates that for a constant thermal reactor power, decreasing the vessel radius decreases the total vapor generator mass, but increases the pressure losses because of the increased length of the tubes needed to maintain a constant heat-transfer area. Similarly, increasing the tube diameter increases the vapor generator mass because of the increased length of the tubes needed to maintain a constant heat-transfer area. Also, increasing the reheater inlet temperature increases the vapor generator mass, since the higher temperature reduces the material strength and

Table 2 Candidate structural materials for the PBRSC

Property	Nb-1Zr	ASTAR-811C	Mo-10Re	W-26Re	ASTAR-1611C/Nicalon
Melting point (K)	2740	3350	2810	3370	3250
Density (Kg/m^3)	8,400	16,700	11,800	19,600	15,500
Thermal conductivity at 1350K (W/m·K)	70	60	70	60	——
Tensile strength at 1350K (MPa)	193	413	310	551	621
Creep strength (MPa)	10.3	69	20.7	82.8	——
DBTT (K)	75	120	140	400	——
Neutron absorption cross section (barns)	0.094	0.334	0.092	0.23	——
Figure of merit (Kg/m^2)[a]	1,508	583	848	——	358

[a]Figure of merit, which is the mass per unit surface area, evaluated at 1/3 the yield strength for maximum strength.

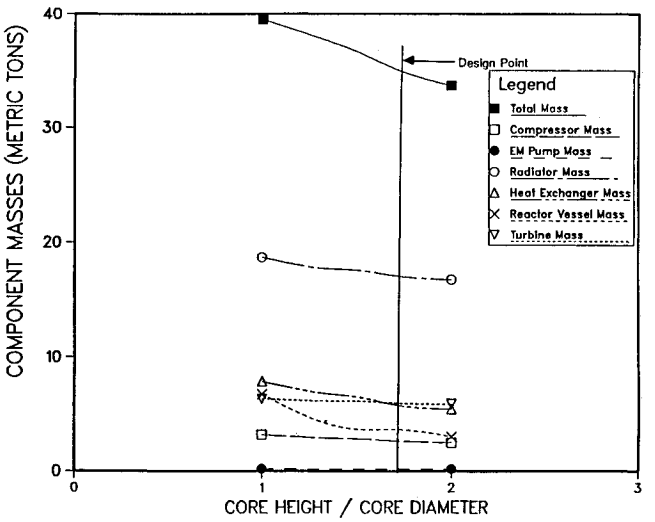

Fig. 8. Effect of the core height-to-diameter ratio on the PBR power module mass.

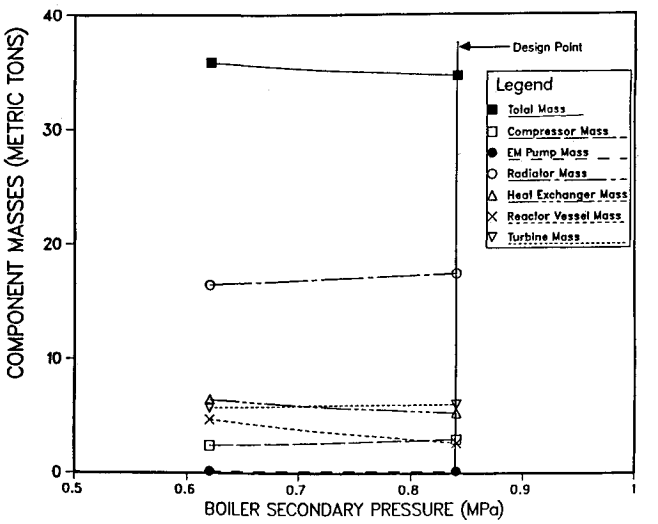

Fig. 10. Effect of the secondary-loop pressure on the PBR power module mass.

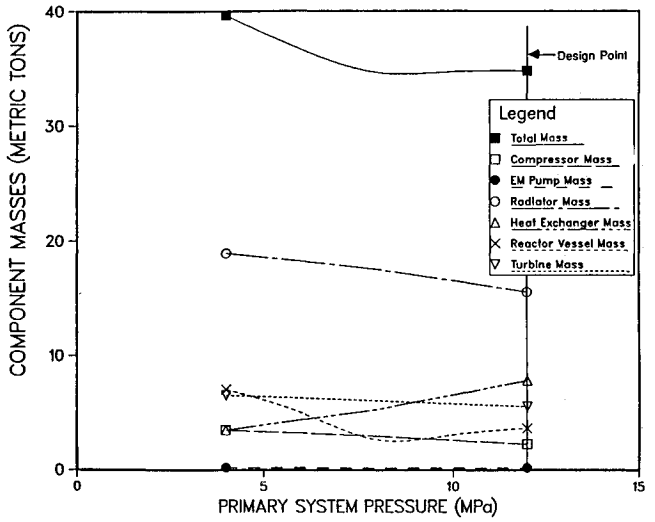

Fig. 9. Effect of the primary-loop pressure on the PBR power module mass.

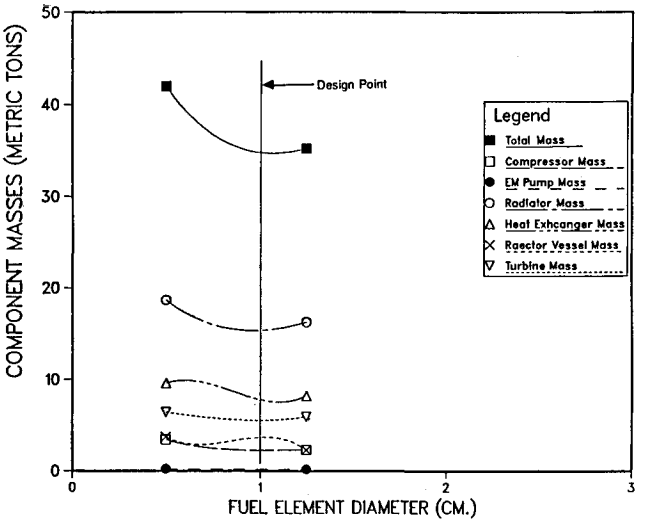

Fig. 11. Effect of the fuel element diameter on the PBR power module mass.

requires thicker walls to withstand the primary system pressure. The vapor generator design with the smallest mass is 3 m high with a vessel radius of 0.62 m, and 40,000, 5-mm-diam tubes.

Materials Selection in the Core and the Vapor Generator Vessel

The high operating temperatures of the PBRSC (1800–2300 K) required a detailed materials selection procedure for the core and the vapor generator vessel. The alloy W-26Re, which has a high melting point and strength, was discarded because of its high ductile-to-brittle transition temperature (DBTT) (see Table 2). The alloy NB-1%ZrC, which has the lowest density, was also excluded because of its low melting point. The alloy ASTAR-811C possesses good physical properties, but was restricted only to the exit frit in the core because of its Hafnium content; Hafnium is a strong neutron absorber. The Mo-10Re was selected for the remaining core structure; however, it was reinforced with Nicalon (a SiC fiber) for use in the reactor pressure vessel. Because the ASTAR-1611C/Nicalon composite has a high melting temperature and high strength at high temperatures, it was selected for fabrication of all vapor generator components.

Power System Mass Optimization and Base System Features

Since the PBR power module is designed for multimodal power requirements, it was optimized first for the burst mode of operation. The overall mass of the power module was minimized by varying the core height-to-diameter ratio, the fuel element diameter, the boiler secondary-loop pressure, the primary-loop pressure, and the high-pressure tubine inlet temperature as functions of the average core volumetric heat-generation rate. The parameters that resulted in the lowest power module mass are core height-to-diameter ratio of 1.7, turbine inlet temperature of 1800 K, primary coolant pressure of 8 MPa, secondary-loop pressure of 0.84 MPa, fuel element diameter of 1 cm, average core volumetric heat-generation rate of 2000 MW/m^3, and ZrC content in fuel kernel of 23% by volume. As shown in Fig. 8, increasing the core height-to-diameter ratio decreases the mass of the system components and the power module's total mass. This decrease in the power module mass is because increasing the core height-to-diameter ratio decreases the core radius, and the pressure losses through the core that in turn reduces the mass of the reactor vessel and the mass and the power of the compressor. The lower compressor power reduces the turbine mechanical work and the heat-

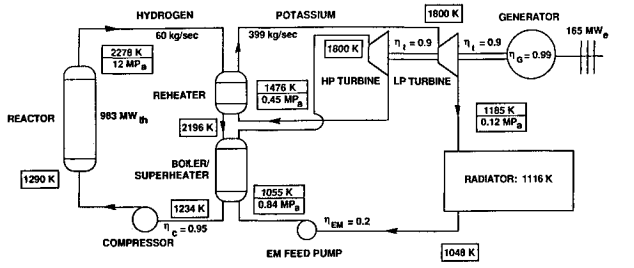

Fig. 12. Line diagram of an integrated PBRSC module during burst mode of operation.

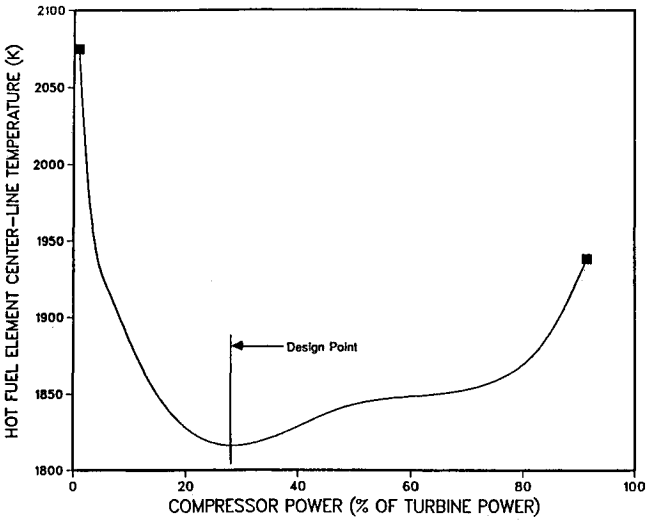

Fig. 13. Effect of compressor power on the maximum fuel element temperature in the reactor core during the alert mode of operation.

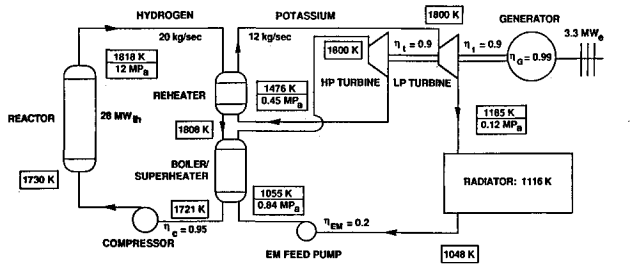

Fig. 14. Line diagram of an integrated PBRSC module during alert mode of operation.

rejection load, resulting in a lower radiator mass. The results also demonstrate that the radiator is the most massive component in the system, followed by the vapor generator and the reactor core. Figure 9 shows that increasing the primary-loop pressure beyond 8 MPa only minimally affects the system's mass. However, for a primary-loop pressure less than 8 MPa, the power module mass decreases as the primary-loop pressure increases. Figure 10 shows that increasing the secondary-loop pressure also decreases the total module mass. This reduction occurs because of the decreased vapor generator mass, but despite the increased radiator mass. Figure 11 shows that a minimum module mass occurs at about 1-cm fuel element diameter, and any deviation from this value causes the module mass to increase. Figure 12 presents a line diagram of an integrated power module showing the optimized operating parameters during the burst mode.

In addition, an optimization of the power module was performed for the alert mode to minimize the maximum fuel temperature and the number of the operating parameters allowed to change between the burst and alert modes; this reduces the transition time from the alert mode to the burst mode. To achieve this goal, all secondary-loop parameters, with the exception of the working fluids mass flow rates, are kept the same in both the alert and the burst modes. The results in Fig. 13 show that during the alert mode the lowest fuel element centerline temperature is achieved at a compressor power that is about 26% of the turbine mechanical power.[2] Any deviation from this value causes the fuel temperature to increase. High compressor power decreases the plant efficiency, causing the core's thermal power and the core and the fuel temperatures to increase. Conversely, decreasing the compressor's power below 26% of the turbine's mechanical power reduces heat-transfer coefficient in the core, causing the fuel temperature to increase. Figure 14 presents a line diagram of the integrated power module showing the optimized operating parameters during the alert mode.

Comparison with other System Configurations

The selected module configurations for the burst and alert modes of operation (Figs. 12 and 14) were compared with several other possible configurations. The results presented in Table 1 demonstrate that the power modules with the highest specific power (3.8 kWe/kg) are the hydrogen-cooled reactor/potassium Rankine cycle (H_2/K) for both alert and burst modes, and the combination of an open-loop Brayton (hydrogen) for burst operation and H_2/K for alert operation. The closed Brayton cycle with a high-pressure turbine inlet temperature of 1800 K gives the lowest specific power (2.2 kWe/kg). Raising this temperature to 2278 K increases the power module's specific power to 3.1 kWe/kg, but the system reliability is reduced, and requires using higher temperature materials for the turbine blades and casing. For the closed-loop Brayton cycle, the compressor's power requirements and, therefore, the turbine's power requirements, are extremely high, resulting in a higher reactor power and higher waste-heat rejection. As a result, the savings in the radiator mass because of the higher conversion efficiency of the closed-loop Brayton cycle (20% vs 17% for potassium Rankine cycle) were offset by the increase caused by the higher heat-rejection load.

Key Research and Development Issues

This study raised several critical technical issues that need further research and development. Fabricating spherical fuel elements with a high packing density of microspheres, developing a procedure for the quality control of the ZrC coating of the microspheres, and investigating long-term irradiation and swelling behavior of the fuel elements at temperatures up to 3200 K are critical issues requiring further research and development. In addition, the migration of uranium metal from the fuel kernel into the ZrC coating at temperatures in excess of 2000 K during the burst mode should be investigated. The refractory metal-ceramic fiber composite concept proposed for fabricating the containment vessels of the reactor and the vapor generator must also be tested. Structural integrity and the vibrations induced during the burst mode are also key issues requiring further investigation. Demonstrating the assembly and welding of tens of thousands of tubes in the vapor generator are also considered key research and development issues. Additionally, more detailed analysis, modeling, and experimental investigations of two-phase flow separation in microgravity environment are needed.

Conclusions

This paper has developed and optimized the design of a power module that uses the pellet bed reactor concept for meet-

ing the multimegawatt power requirements of some of the SDI missions during both alert and burst modes of operation. Results show that the specific power of the hydrogen-cooled PBR/potassium Rankine cycle system (3.8 KWe/kg) is superior to that of the closed-loop Brayton cycle system (3.1 KWe/kg), but competitive with that of the open-loop Brayton cycle system (3.8 KWe/kg) if liquid hydrogen has to be carried onboard. In addition, this study demonstrated that the radiator, composing 44% of the power module mass, is the most massive component; in contrast, the reactor itself is only 10% of the power module mass, whereas the vapor generator mass is 27%. The vapor generator mass was reduced by lowering the compressor pumping power; over 20% of the turbine's mechanical power is used to drive the primary-loop compressor. Therefore, for a given electric power output, lower primary-loop pressure losses in the reactor core reduce the compressor power, turbine size, reactor thermal power, radiator mass, and as a result, consequently reduce the overall power module mass. In conclusion, a design effort geared toward a core configuration with low-pressure losses and low radiator mass should yield a low overall power module mass.

Acknowledgments

This work was done jointly by the University of New Mexico's Institute for Space Nuclear Power Studies and the Science Application International Corporation for the U.S. Department of Energy under Contract No. DE-AC03-86SF16508.

References

[1]Kirpich, A., Biddiscombe, R., Chan, J., and McNamara, E., "Comparison of Concepts for a 300 KWe Nuclear Power System," *Proceedings of the 21st IECEC Meeting*, American Chemical Society, Washington, D.C., Vol. 3, Paper No. 869434, 1986, pp. 1933–1937.

[2]Buden, D., El-Genk, M., Parlos, A., Mims, J., McGhee, J., and Lapin, S., "Pellet Bed Reactor Concept," Final Report prepared for the U.S. Dept. of Energy, San Francisco, CA, DE-AC03-86SF16508, May 1987.

[3]El-Genk, M. S., Parlos, A. G., McGhee, J. M., Lapin, S., Buden, D., and Mims, J., "Pellet Bed Reactor Design for Space Power," AIAA Paper 87-9360.

[4]Nabielek, H., et al., "Fuel for Pebble-Bed HTRs," *Journal of Nuclear Engineering and Design*, Vol. 78, 1984, pp. 155–166.

[5]Buden, D. and Mims, J., "Multi-Modal Nuclear Power Plant with Reuseable Fluid Recovery for Pulse Power," Final Report prepared for the U.S. Dept. of Energy, San Francisco, CA, Sept. 1986.

[6]Koening, D. R., *Experience Gained from the Space Nuclear Rocket Program (Rover)*, Los Alamos National Lab. Report, LA-10062-4, Los Alamos, NM, 1986.

[7]Longer, S. "Physicochemical Properties of Carbides for Nuclear Applications," *Materials and Fuels for High Temperature Nuclear Energy Applications*, M. T. Simnod and L. R. Zumwelt, eds., 1964.

[8]Stansfield, O. M., Noman, F. J., Simon, W. A., and Turner, R. F., *Interaction of Fission Products and SiC in TRISO Fuel Particles: A Limiting HTGR Design Parameter*, U.S. Dept. of Energy, San Francisco, CA, Rept. No. GA-A17183-UC-77, 1983.

[9]Incropera, F. P. and DeWitt, D. P., *Fundamentals of Heat Transfer*, John Wiley and Sons, New York, 1981.

[10]Koae, J., private communication, General Atomics Technology, Jan. 1987.

[11]El-Genk, M. S. and Moore, R. L., "Transient Debris Freezing and Potential Well Melting During a Severe RIA Experiment," *Journal of Nuclear Technology*, Vol. 53, June 1981, pp. 354–373.

[12]Lapple, C. E., "Dust and Mist Collection," *Chemical Engineer's Handbook*, 5th ed., J. H. Perry, ed., McGraw-Hill, New York, 1973.

[13]Gupta, S. N., Chaube, R. B., and UPadhyay, S. N., "Fluid-Particle Heat Transfer in Fixcol and Fluidized Bed," *Journal of Chemical Engineering Science.*, Vol. 29, 1974, pp. 839–843.

[14]Van Wyler, G. J. and Sonntag, R. E., *Fundamentals of Classical Thermodynamics*, John Wiley and Sons, New York, 1973.

[15]Alcouffe, R. E., Brinkley, F. W., Marr, D. R., and O'Bell, R. D., *User's Guide for TWODANT: A Code Package for Two-Dimensional, Diffusion-Accelerated, Neutral-Particle Transport*, Los Alamos National Lab. Report, Los Alamos, NM, LA-10049-M, Rev. 1, UC-32, 1984.

[16]Rust, J. M., *Nuclear Power Plant Engineering*, Haralson Publishing Co., Buchanan, Georgia, 1979.

[17]Weisman, J., *Elements of Nuclear Reactor Design*, R. E. Krieger Publishing Co., Molabar, FL, 1983.

[18]Frass, A. P. and Ozisik, M. N., *Heat Exchanger Design*, John Wiley and Sons, New York, 1965.